J|A|C|S ARTICLES

Published on Web 10/21/2009

Synthesis of Highly Antibacterial Nanocrystalline Trivalent Silver Polydiguanide

Sukdeb Pal, Eun Jeong Yoon, Yu Kyung Tak, Eung Chil Choi, and Joon Myong Song*

Research Institute of Pharmaceutical Sciences and College of Pharmacy, Seoul National University, Seoul, 151-742, South Korea

Received June 22, 2009; E-mail: jmsong@snu.ac.kr

Abstract: Highly monodispersed nanoparticles of a trivalent silver polydiguanide complex are synthesized by oxidation of the monovalent silver, followed by stabilization of the oxidized higher-valent metal through complexation with a polydiguanide ligand in a reverse microemulsion at room temperature. The synthesized nanoparticles have excellent photostability and displayed superior antibacterial activity toward Gram-positive and Gram-negative prokaryotes of clinical interest *in vitro* compared to silver sulfadiazine. These nanoparticles may serve as a new generation antibacterial metallopharmaceutical in wound care.

Introduction

Burn wounds, especially large burn wounds, are a critical threat to burn victims, causing dehydration, systemic infection, and other complications.[1−4] The use of antibacterial agents locally or systemically inhibits microorganism growth around the wound, allowing a suitable microenvironment for healing.[5] The application of silver and its salts in the treatment of burn wounds is thus of special interest[6,7] and has prompted an upsurge in research on the synthesis of silver(I) complexes with projected antibacterial application.[8−11] The antibacterial performance of ionic silver[12] is correlated to its valence form, and it has been found that the high valence silver ion exhibits stronger and more effective antibacterial action than the low valence ion.[7,13−15] Although the antibacterial performance of the different silver valence varies in treating heterogeneous bacteria, the general consensus is that the antibacterial activity of higher valence silver is greater than that of the lower one. However, silver nitrate and other complexes including silver sulfadiazine, the most widely used topical antibacterial agent in the treatment of burn wounds, are essentially monovalent silver antibacterial agents.

Encouraging results have recently been reported regarding the bactericidal activity of silver nanoparticles of either simple or composite nature.[16−23] We have demonstrated that in addition to size dependent interactions, silver nanoparticles also undergo shape-dependent interactions with gram-negative bacteria.[24] The high surface to volume ratio of nanoparticles ensures that a significantly large surface area of the particle is in contact with the bacteria. In fact results from earlier work demonstrated increased the antimicrobial effectiveness of a smaller particle size silver sulfadiazine product and stabilization of these smaller particles by adsorbed surfactant.[25,26] Encouraged by this finding and by the pressing interest in developing nanosilver-based

(1) Atiyeh, B. S.; Hayek, S. N.; Gunn, S. W. *Burns* **2005**, *31*, 944–956.
(2) Atiyeh, B. S.; Gunn, S. W.; Hayek, S. N. *World J. Surg* **2005**, *29*, 131–148.
(3) Connor-Ballard, P. A. *Am. J. Nurs.* **2009**, *109*, 48–56.
(4) Connor-Ballard, P. A. *Am. J. Nurs.* **2009**, *109*, 54–62.
(5) Lansdown, A. B.; Williams, A.; Chandler, S.; Benfield, S. *J. Wound Care* **2005**, *14*, 155–160.
(6) Church, D.; Elsayed, S.; Reid, O.; Winston, B. D.; Lindsays, R. *Clin. Microbiol. Rev.* **2006**, *19*, 403–434.
(7) Atiyeh, B. S.; Costagliola, M.; Hayek, S. N.; Dibo, S. A. *Burns* **2007**, *33*, 139–148.
(8) Melaiye, A.; Simons, R. S.; Milsted, A.; Pingitore, F.; Wesdemiotis, C.; Tessier, C. A.; Youngs, W. J. *J. Med. Chem.* **2004**, *47*, 973–977.
(9) Dias, H.V. R.; Batdorf, K. H.; Fianchini, M.; Diyabalanage, H. V. K.; Carnahan, S.; Mulcahy, R.; Rabiee, A.; Nelson, K.; van Waasbergen, L. G. *J. Inorg. Biochem.* **2006**, *100*, 158–160.
(10) Ray, S.; Mohan, R.; Singh, J. K.; Samantaray, M. K.; Shaikh, M. M.; Panda, D.; Ghosh, P. *J. Am. Chem. Soc.* **2007**, *129*, 15042–15053.
(11) Hindi, K. M.; Siciliano, T. J.; Durmus, S.; Panzner, M. J.; Medvetz, D. A.; Reddy, D. V.; Hogue, L. A.; Hovis, C. E.; Hilliard, J. K.; Mallet, R. J.; Tessier, C. A.; Cannon, C. L.; Youngs, W. J. *J. Med. Chem.* **2008**, *51*, 1577–1583.
(12) Melaiye, A.; Sun, Z.; Hindi, K.; Milsted, A.; Ely, D.; Reneker, D.; Tessier, C.; Youngs, W. *J. Am. Chem. Soc.* **2005**, *127*, 2285–2291.
(13) Djokic, S. S. *J. Electrochem. Soc.* **2004**, *151*, C359–C364.
(14) Dellasega, D.; Facibeni, A.; Di Fonzo, F.; Bogana, M.; Polissi, A.; Conti, C.; Ducati, C.; Casari, C. S.; Bassi, A. L.; Bottani, C. E. *Nanotechnology* **2008**, *19*, 475602.
(15) Zhao, J.; Zhang, W.; Wang, G. *US Pat. Appl.* **2007**; 0042052.
(16) Liong, M.; France, B.; Bradley, K. A.; Zink, J. I. *Adv. Mater.* **2009**, *21*, 1684–1689.
(17) Balogh, L.; Swanson, D. R.; Tomalia, D. A.; Hagnauer, G. L.; McManus, A. T. *Nano Lett.* **2001**, *1*, 18–21.
(18) Lee, H. Y.; Park, H. K.; Lee, Y. M.; Kim, K.; Park, S. B. *Chem. Commun.* **2007**, 2959–2961.
(19) Oyanedel-Craver, V. A.; Smith, J. A. *Environ. Sci. Technol.* **2008**, *42*, 927–933.
(20) Loher, S.; Schneider, O. D.; Maienfisch, T.; Bokorny, S.; Stark, W. J. *Small* **2008**, *4*, 824–832.
(21) Schneider, O. D.; Loher, S.; Brunner, T. J.; Schimidlin, P.; Stark, W. J. *J. Mater. Chem.* **2008**, *18*, 2679–2684.
(22) Sambhy, V.; MacBride, M. M.; Peterson, B. R.; Sen, A. *J. Am. Chem. Soc.* **2006**, *128*, 9798–9808.
(23) Gunawan, C.; Teoh, W. Y.; Marquis, C. P.; Lifia, J.; Amal, R. *Small* **2009**, *5*, 341–344.
(24) Pal, S.; Tak, Y. K.; Song, J. M. *Appl. Environ. Microbiol.* **2007**, *73*, 1712–1720.
(25) Kolling, W. M. *Studies on silver sulfadiazine poloxamer 407 gels*; University of Illinois: Chicago, 1984.
(26) Kaur, M. A. *in The effect of formulation excipients on the crystal growth and habit of silver sulfadiazine*; University of Mississippi: Oxford, 2000.

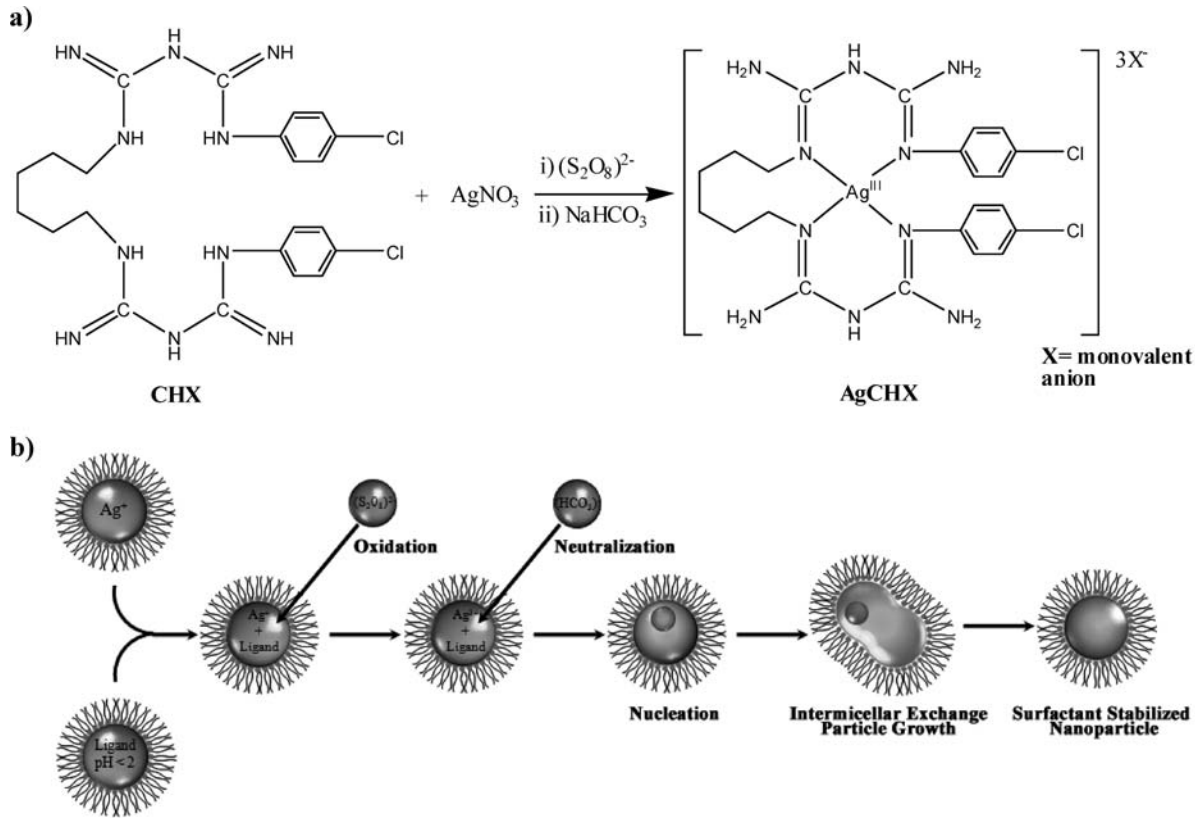

Figure 1. (a) Structure of chlorhexidine and proposed structure of AgCHX. (b) Schematic presentation of the sequences involved in the synthesis of AgCHX nanoparticles in reverse microemulsion.

antimicrobials active against resistant organisms, we thought that further size reduction of a higher valent silver-based antibacterial agent would result in greater antimicrobial effectiveness. Moreover, since antibacterial agents are used as a cream or paste or in wound dressings, monodispersed antibacterial nanoparticles would improve the homogeneous and uniform distribution of the active agent in the host matrix. However, smallness in itself is not the goal. Synthesis and characterization of higher valent silver-based nanoscaled materials in terms of increased stability under ambient temperature, pressure, and light; good hydration; and sustained release of silver ions with increased concentration at the wound surfaces will play key roles in burn care.

Because of poor stability, complexes of Ag(III) are rare and much more restricted than those of Ag(II).[27] This is reflected by the fact that, so far, X-ray crystallographic structural characterization has been obtained for only a few silver(III) organometallic complexes with biguanides, corroles, and carboporphyrins.[28−30] Recently imine-oxime ligands have also been shown to be good ligands for the stabilization of uncommon high oxidation states of silver.[31] But these complexes are not photostable and, like *N*-heterocyclic carbene silver(I) complexes, decompose in aqueous solutions.[32,33]

Interestingly, biguanide or substituted biguanide, such as ethylenebiguanide, forms quadricovalent cationic complexes with silver(III) that are stable (including photostable) in ambient conditions. Like the biguanide molecule, polydiguanides also possess conjugate single and double bond systems and filled π-type delocalized orbitals suitable for higher valent silver complex formation. For this reason, we chose a commonly used symmetric polydiguanide molecule, chlorhexidine, 1,1′-hexamethylene-bis-5-(4-chlorophenyl)biguanide, with two ionizable guanide moieties (Figure 1a) as the ligand to synthesize a stable nanocrystalline silver(III) complex. It is also an important antiseptic, disinfectant, pharmaceutical and cosmetic preservative, and antiplaque agent.

The wet chemical preparation of silver(III) polydiguanide can be realized by oxidizing a mixture of a biguanide base or its normal salt and silver nitrate solution in feebly acidic or neutral medium. However, this preparative method does not allow controlling the size of the final crystalline product. To attempt the challenge of synthesizing nanocrystalline silver(III) chlorhexidine (AgCHX) (Figure 1a) we developed a simple but novel approach based upon oxidation of silver and stabilization of the oxidized higher valent silver through complexation with polydiguanide in a reverse microemulsion. Water-in-oil (W/O) reverse microemulsion can be defined as a thermodynamically stable, isotropic, and transparent solution of oil, water, and surfactant. The water droplets, dispersed as nanosized liquid entities in a continuous domain of oil, provide a favorable

(27) Levason, W.; Spicer, M. D. *Coord. Chem. Rev.* **1987**, *76*, 45–120.
(28) Kunchur, N. R. *Nature* **1968**, *217*, 539–541.
(29) Bruckner, C.; Barta, C. A.; Brinas, R. P.; Krause Bauer, J. A. *Inorg. Chem.* **2003**, *42*, 1673–1680.
(30) Lash, T. D.; Colby, D. A.; Szczepura, L. F. *Inorg. Chem.* **2004**, *43*, 5258–5267.
(31) Eltayeb, M. A.; Sulfab, Y. *Polyhedron* **2007**, *26*, 39–42.
(32) Garrison, J.; Youngs, W. *Chem. Rev.* **2005**, *105*, 3978–4008.
(33) Kascatan-Nebioglu, A.; Melaiye, A.; Hindi, K.; Durmus, S.; Panzner, M.; Hogue, L.; Mallett, R.; Coughenour, C.; Hovis, M.; Crosby, S.; Milsted, A.; Ely, D.; Tessier, C.; Cannon, C.; Youngs, W. *J. Med. Chem.* **2006**, *49*, 6811–6818.

microenvironment for controlling the chemical reaction. Particle size and shape can be simply controlled by varying microemulsion parameters.[34,35] Microemulsion technique has been widely used to prepare inorganic (metal and metal salts) and organic nanoparticles,[34−39] hollow spheres,[40] and silica and modified silica nanoparticles.[41,42] Surprisingly, this method, to the best of our knowledge, has never been verified for synthesis of nanocrystalline organometallic complexes of noble metals wherein the metal is stabilized in an uncommonly high oxidation state. Here, we report, for the first time, synthesis of a nanocrystalline AgCHX complex in reverse microemulsion, demonstrating its flexibility for complexation reaction and the fabrication of essentially monodispersed nanoparticles of higher valent metal complex. We also report herein that synthesized AgCHX showed strong antibacterial activity against the tested Gram (+)/(−) and methicillin-resistant *Stahylococcus aureus* (MRSA) strains. The minimal inhibitory concentrations (MICs) of nanocrystalline Ag(III)CHX were much lower than those of the ligand (CHX), $AgNO_3$, and the gold standard, silver sulfadiazine.

Experimental Section

The W/O microemulsion was established by dissolving AOT (sodium salt, 0.1 M) in heptane (10 mL) followed by addition of aqueous solutions of the reagents (silver nitrate, CHX, sodium peroxydisulfate at a molar ratio of 1:1:2, and saturated solution of $NaHCO_3$). The volume of each reactant varied with the water to surfactant molar ratio (R). The concentrations of $AgNO_3$ given in the text were based on the volume of aqueous solution rather than the total volume. To reach a finer and more stable state of the microemulsion, an ultrasonic bath was used.

Transmission Electron Microscope Analysis. The size and morphology of AgCHX nanoparticles synthesized in a W/O microemulsion were measured using a transmission electron microscope (JEM 3010 (HR) and JEM 1010, Jeol, Tokyo, Japan). The sample for TEM was prepared by placing a drop of the nanoparticle-containing microemulsion on 200-mesh carbon-coated copper grids.

X-ray Photoelectron Spectroscopy. Surface chemistry was analyzed by XPS (Sigma Probe, Thermo-VG, UK) with a monochromatic Al Kα (1486.7 eV) X-ray source. Survey XPS data were acquired over 1200 eV in Constant Analyzer Energy mode with a pass energy of 30 eV and a resolution of 0.1 eV.

Zeta Potential Measurement. The zeta potentials of the nanoparticles, synthesized at R values of 8, 10, 12.4, and 15 ($AgNO_3$ solution concentration was 5 mm), were measured using an electrophoretic light scattering spectrophotometer (ELS 8000, Otsuka Electronics, Osaka, Japan).

Bacterial Strains and Culture Conditions. The test organisms include four strains of Gram-negative bacteria (*Acinetobacter calcoaceticus* (ATCC 23055), *Citrobacter freundii* (ATCC 6750), *Klebsiella pneumonia* (ATCC 10031), and *Pseudomonas aeruginosa* (ATCC 27853)); four strains of Gram-positive bacteria (*Enterococcus faecalis* (ATCC 29212), *Staphylococcus aureus* (ATCC 25923), *Staphylococcus epidermidis* (ATCC 12228), *Propionibacterium acnes* (ATCC 6919)); and seven strains of MRSA obtained from patients in 2007. All challenge bacterial strains were obtained from American Type Culture Collection (Rockville, MD, USA) except *P. acnes* ATCC 6919 which was provided by Korean Collection for Type Cultures (Daejon, Korea). All tests were performed in line with Clinical and Laboratory Standards Institute (formerly National Committee for Clinical Laboratory Standard, NCCLS) guidelines.[43]

The overnight cultures served as the inocula for experiments. Unless otherwise stated, the strains were grown overnight in Tryptic Soy broth or agar (TSB or TSA, Difco Laboratories, Detroit, MI, USA) at 37 °C under aerobic conditions. *P. acnes* ATCC 6919 inocula were cultured in Brain Heart Infusion broth or agar (BHI, Difco Laboratories, Detroit, MI, USA) supplemented with 1% glucose (BHIG) grown for 48 h at 37 °C under anaerobic conditions created by the GasPak jar system (BBL Microbiology Systems, Cockeysville, MD).

Determination of MICs and MBCs and IC_{50}s. MICs were determined by the agar dilution method in BHI agar for *P. acnes* or in Mueller Hinton agar (MH, Difco Laboratories, Detroit, MI, USA) for all other species, using a multipoint inoculator. Plates were read after incubation at 37 °C for 48 h under anaerobic conditions (GasPak) for *P. acnes* or for 24 h in air for all other species. To determine the MICs by the broth microdilution method, Mueller Hinton broth (MH, Difco Laboratories, Detroit, MI, USA) was used for all bacterial strains except for *P. acnes* ATCC 6919, which was grown in BHI broth supplemented with 1% glucose. Strains were cultured in 96-well microplates. To evaluate the inhibitory effects of the antibacterial agents on bacterial growth, each well was supplemented with a range of concentrations of the active agents. Following 24 h of incubation in air or 48 h of incubation in a GasPak jar system at 37 °C, the wells were inspected for microbial growth and the MIC was determined as the lowest concentration that did not produce visual growth. An uninoculated set was also incubated to know the coagulation effect. The minimum bactericidal concentrations (MBCs) were determined by reinoculation of each growth in wells into empty MH agar or BHI agar plates. After 24 or 48 h of incubation, MBC was defined as the lowest concentration at which no growth was observed on the plate. All tests were performed in triplicate. IC_{50}s were determined by plotting the percent inhibition of bacterial growth determined by turbidity measurement against the concentration of the tested compounds.

Results and Discussion

An illustration of the sequences involved in the synthesis of AgCHX nanoparticles in reverse microemulsion is shown in Figure 1b. There are three key steps for the formation of AgCHX nanoparticles inside microemulsions. The first one is to make the ligand water-soluble. Chlorhexidine (the free base) is essentially water insoluble and only exists at very low hydrogen ion concentrations (pH > 12). CHX is used as the salt form, commercially available as CHX diacetate, dihydrochloride, or digluconate. However, from the viewpoint of unwanted interaction of the metal ion with other organic and inorganic species and coprecipitation, these salts are not suitable as a ligand source. Taking advantage of the pK_a values of CHX (2.2 and 10.3) which make it dicationic over the entire range of

(34) Lopez-Quintela, M. A. *Curr. Opin. Colloid Interface Sci.* **2003**, *8*, 137–144.
(35) Destrée, C.; Nagy, J. B. *Adv. Colloid Interface Sci.* **2006**, *123*, 353–367.
(36) Ersen, O.; Bégin, S.; Houllé, M.; Amadou, J.; Janowska, I.; Grenêche, J. -M.; Crucifix, C.; Pham-Huu, C. *Nano Lett.* **2008**, *8*, 1033–1040.
(37) Taylor, K. M. L.; Rieter, W. J.; Lin, W. *J. Am. Chem. Soc.* **2008**, *130*, 14358–14359.
(38) Zhang, P.; Guo, Y. *J. Am. Chem. Soc.* **2009**, *131*, 3808–3809.
(39) Muddana, H. S.; Morgan, T. T.; Adair, J. H.; Butler, P. J. *Nano Lett.* **2009**, *9*, 1559–1566.
(40) Zimmermann, C.; Feldmann, C.; Wanner, M.; Gerthsen, D. *Small* **2007**, *3*, 1347–1349.
(41) Lu, C.-W.; Hung, Y.; Hsiao, J.-K.; Yao, M.; Chung, T.-H.; Lin, Y.-S.; Wu, S.-H.; Hsu, S.-C.; Liu, H.-M.; Mou, C.-Y.; Yang, C.-S.; Huang, D.-M.; Chen, Y.-C. *Nano Lett.* **2007**, *7*, 149–154.
(42) Zanarini, S.; Rampazzo, E.; Ciana, L. D.; Marcaccio, M.; Marzocchi, E.; Montalti, M.; Paolucci, F.; Prodi, L. *J. Am. Chem. Soc.* **2009**, *131*, 2260–2267.
(43) NCCLS, National Committee for Clinical Laboratory Standards. Methods for dilution antimicrobial susceptibility tests for bacteria that grow aerobically. Approved Standard-Fifth Edition, M7-A5. Wayne, PA: NCCLS, 2000.

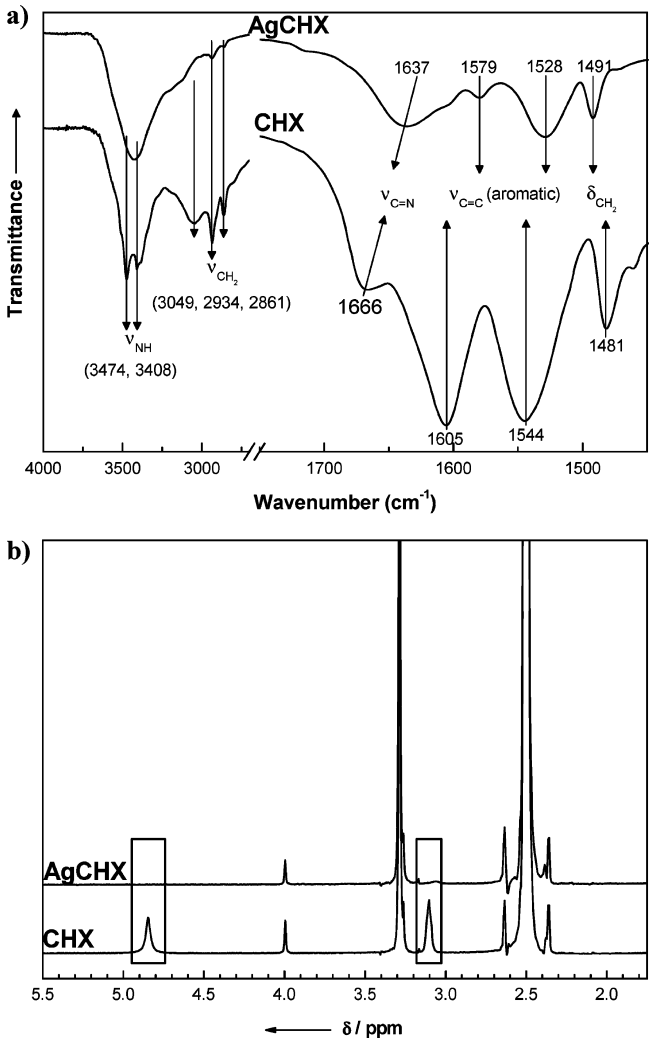

Figure 2. (a) IR spectra of chlorhexidine and synthesized AgCHX nanoparticles. (b) ^{1}H NMR spectra of chlorhexidine and synthesized AgCHX nanoparticles.

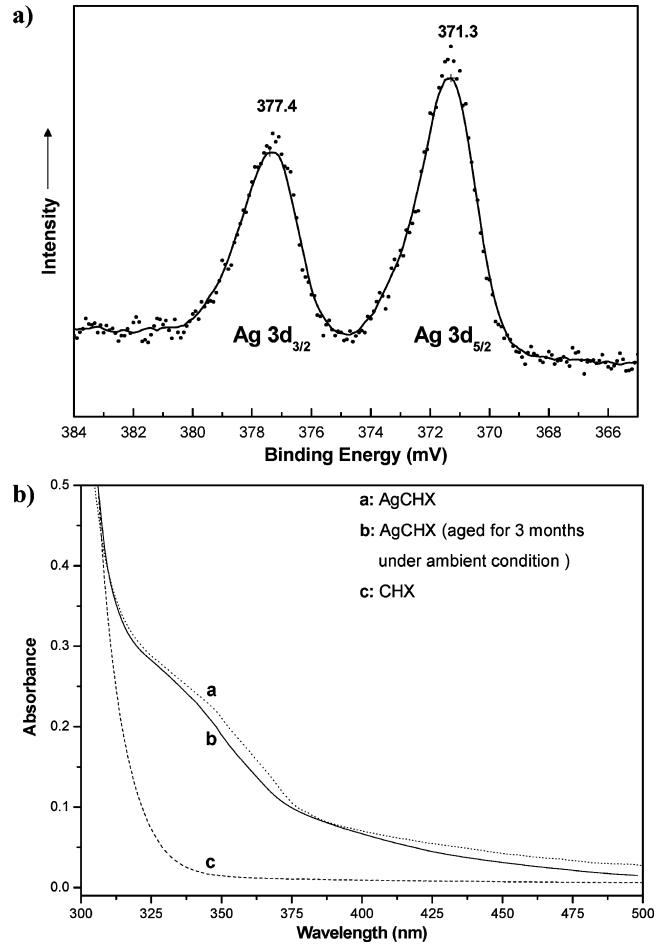

Figure 3. (a) Silver $3d_{3/2}$ and $3d_{5/2}$ spectra of AgCHX nanoparticles. (b) UV−visible spectra of CHX and AgCHX nanoparticles.

physiological pH,[44] the solublization of CHX in water is achieved by forming a dihydrogensulfate salt of CHX in weak sulfuric acid. The second important step is to oxidize Ag^+ to Ag^{3+}. In the presumed silver(I) complex some of the *d* electrons of the Ag^+ ion must be forced to occupy higher-energy antibonding orbitals, from which they can be removed by peroxydisulfate oxidation to produce a trivalent silver complex. The third step is to provide the feebly acidic or neutral medium most appropriate for complexation and coprecipitation by addition of bicarbonate.

The microemulsion compositions were selected according to the phase diagram of the ternary system of water/dioctyl sulfosuccinate (AOT)/heptane. The smaller headgroup area of AOT compared to the volume of the hydrocarbon tail and the wedge-shaped geometry favor the formation of reverse micelles with a spherical droplet structure as evident from the spherical geometry found in the entire single-phase microemulsion zone of the phase diagram for AOT and various organic solvent-based microemulsion systems.[45]

FTIR and ^{1}H NMR spectra of CHX and AgCHX are depicted in Figure 2. FTIR and ^{1}H NMR studies show that binding is due to the interaction between the nitrogen of the −N(H)− bond of CHX and silver. The characteristic stretching bands at 3474 and 3408 cm^{-1} for −N(H)− appeared as a single band in the complex. The absence of signal at 4.84 ppm in the complex provides further support in favor of this bonding mode. LC-MS (ESI) results suggest a 1:1 stoichiometric ratio between metal and ligand (peak for $[M + H]^+$, where M = $Ag(C_{22}H_{30}Cl_2N_{10})$).

For chlorhexidine, IR (KBr): ν = 3474 (s), 3408(s; ν (−NH−)), 3049 (w), 2934(m), 2861 (w; ν (CH_2)), 1666 (w; ν (C═N)), 1605 (s), 1544 (s; ν (C═C aromatic)), 1481 cm^{-1} (m; δ (CH_2); ^{1}H NMR (500 MHz, DMSO-d_6, δ): 7.19 (d, 4H, Ar H), 6.79 (d, 4H, 2H; Ar H), 4.84 (s, 2H; Ar C−NH), 3.99 (s, 4H, C═NH), 3.10 (s, 4H, NH), 1.44 (4H, CH_2), 1.31 (4H, CH_2), 1.23 (4H, CH_2). For silver(III) chlorhexidine complex, IR (KBr): ν = 2934 (w), 2861 (w; ν (CH_2)), 1637 (w; ν (C═N)), 1579 (w), 1528 (m; ν (C═C aromatic)), 1491 cm^{-1} (m; δ (CH_2); ^{1}H NMR (500 MHz, DMSO-d_6, δ): 7.35 (8H, Ar H), 3.99 (s, NH_2), 1.44 (4H, CH_2), 1.25 (4H, CH_2), 1.14 (4H, CH_2). LC-MS (ESI, *m*/*z*): $[M + H]^+$ calcd for $Ag(C_{22}H_{30}Cl_2N_{10})$, 613.9; found, 613.9. Anal. Calcd for $[Ag(C_{22}H_{30}Cl_2N_{10})](OH)_3$: Ag, 16.25; C, 39.77; H, 4.97; N, 21.09. Found: Ag, 16.22; C, 39.81; H, 4.95; N, 21.15.

(44) Nerurkar, M. J.; Zentner, G. M.; Rytting, J. H. *J. Controlled Release* **1995**, *33*, 357–363.
(45) Fletcher, P. D. I.; Howe, A. M.; Robinson, B. H. *J. Chem. Soc., Faraday Trans. 1* **1987**, *83*, 985.
(46) Bagwe, R. P.; Yang, C.; Hilliard, L. R.; Tan, W. *Langmuir* **2004**, *20*, 8336–8342.

Table 1. Effect of $AgNO_3$ Concentration on the Occupancy Number and the Average Particle Size

R [a]	microemulsion composition (wt%) water/AOT/ heptane	AOT/heptane (wt%/wt%)	AOT/water (wt%/wt%)	$AgNO_3$ (mM)	d [b] (nm)	σ [c]	λ [d]
15	4.0/6.0/90.0	0.07	1.5	10.0	21.20	6.42	32.14
”	”	”	”	7.5	5.96	2.79	24.10
”	”	”	”	5.0	4.17	1.04	16.07
”	”	”	”	2.5	4.14	0.96	8.03
”	”	”	”	1.0	3.95	0.74	3.21

[a] R = water to surfactant molar ratio. [b] d = number average particle diameter. [c] σ = standard deviation. [d] λ = mean number of Ag^+ ions per water core.

The oxidation state of Ag in AgCHX was investigated by Ag 3d X-ray photoelectron spectroscopy (XPS). The XPS binding energy is mostly determined by the oxidation state of the studied atom but could also be influenced by its chemical environment. From the measurements of Ag 3d XPS spectra for AgCHX (Figure 3a), the Ag $3d_{3/2}$ and Ag $3d_{5/2}$ XPS peaks were observed at 377.4 and 371.3 eV, respectively, which fall in the range of literature values for Ag^{3+}.[29] Figure 3b shows the UV−visible spectra of CHX and AgCHX nanoparticles.

The precipitation of AgCHX complex in the microemulsion droplet was achieved by neutralization of the acidic pH with a calculated amount of saturated aqueous solution of $NaHCO_3$. Hydrolyzable salts reduce the size of the effective polar region of the surfactant by screening the electrostatic repulsion between the head groups and, thus, cause an increase in the curvature and rigidity of surfactant aggregates. The shorter equilibrium distance of the head groups results in a tightly packed surfactant layer. Therefore, we speculate that addition of $NaHCO_3$ increases the rigidity of the surfactant shell and may in turn affect the particle formation. However, it should also be noted that the effect of added cation on particle formation is more severe for higher ratios of charge to hydrated cation size. The higher the valence and the smaller the size of the hydrated cation, the higher the screening effect will be on electrostatic repulsion between the surfactant head groups. Na^+, being a monovalent cation and having a high hydrodynamic radius, is expected to produce a moderate effect on the rigidity of the surfactant shell. To realize what happens if the pH is not neutralized, we tried to synthesize AgCHX nanoparticles in microemulsions with R values of 8, 10, 12.4, and 15. The $AgNO_3$ solution concentration was 5 mM. The TEM observation could not be performed as the acidic pH of the droplets adversely affected the copper grids. Also, after 1 day, the microemulsion solution became unstable and phase separation occurred. This is a useful finding that suggests that addition of a bicarbonate solution in the process of AgCHX nanoparticle formation in a reverse micellar system has dual effects. First, it triggers the nucleation process by neutralizing the pH of the water droplets, and second, it imparts enhanced thermodynamic stability to the microemulsions. In fact, upon addition of $NaHCO_3$, the microemulsions (R = 8, 10, 12.4, 15; $AgNO_3$ 5 mM) were stable for more than 3 months.

The effect of silver ion concentration on the size of AgCHX nanoparticles was investigated in the microemulsion system of water/AOT/heptane (4/6/90). The main steps of formation of AgCHX nanoparticles inside microemulsions can be envisioned as follows: (1) oxidation of Ag^+ to Ag^{3+}; (2) stabilization of Ag^{3+} by the complexation with ligand molecules; (3) pH neutralization by addition of bicarbonate and nucleation; and (4) particle growth. We found that increasing the concentration of $AgNO_3$ from 1 to 7.5 mM, with a constant peroxydisulfate to Ag^+ mole ratio ($[(S_2O_8)^{2-}]/[Ag^+] = 2$), did not change the particle size and monodispersity of the nanoparticles (Table 1). Figure 4 shows TEM micrographs of AgCHX nanoparticles with increasing concentrations of $AgNO_3$. It can be seen from the micrograph that the particle size and polydispersity decreased from 21.2 to 5.96 nm and from 6.42 to 2.79 nm, respectively, when the silver(I) ion concentration was decreased from 10 to 7.5 mM (Table 1). The phenomena observed in this study are probably related to the differences in the oxidation, neutralization−nucleation, and growth processes. The rates of both nucleation and growth are dictated mainly by the probabilities of collisions between different reacting entities. While the collision between several ions is related to nucleation, that between one ion and a nucleus or between two or more nuclei is related to the growth process. Considering that the resultant particles are monodispersed and that the size of the resultant particles is determined by the number of the nuclei formed at the very beginning of the neutralization, it can be deduced that the probability of effective collision between one ion and a nucleus was higher than those of the other two collisions. Therefore, when the oxidation was so large that almost all ions were oxidized before the formation of nuclei, the number of nuclei formed was determined by the number of total ions, their distribution in microemulsions, and the collision energy and sticking coefficient for nucleation. At this point, we may consider three distinct possibilities with reference to the difference in the oxidation, nucleation, and growth processes: (1) if $r_{N_n} > r_{N_i}$, (2) if $r_{N_n} \infty r_{N_i}$, and (3) if $r_{N_n} \leq r_{N_i}$, where r_{N_n} and r_{N_i} is the rate of increase of the number of nuclei and total ions, respectively. In the first condition when the number of nuclei increases faster than that of total ions, smaller particles would be obtained. In the second case, the particle size might remain unchanged, while if the third condition prevails, the particle size would become larger with increasing ion concentration. While formation of monodispersed smaller particles at low ion concentration might refer to the first possibility, formation of larger particles at high $AgNO_3$ concentration could belong to the third condition. As observed in this study, the effect of $AgNO_3$ concentration (<7.5 mM) on the size of AgCHX nanoparticles might be attributed to the second condition.

The final particle size is a function of the water core size, the water to surfactant molar ratio (R), the ion occupancy number, the concentration of the reactant species, and the intermicellar exchange coefficient.[33,45] For a given R value, the radius of water core r (in Å) can be estimated as $1.8R + 4.5$.[47] The radius of water core estimated using this relationship was in good agreement with the radius experimentally obtained using

(47) Eastoe, J.; Robinson, B. H.; Visser, A. J. W. G.; Steytler, D. C. *J. Chem. Soc., Faraday Trans.* **1991**, *87*, 1899.

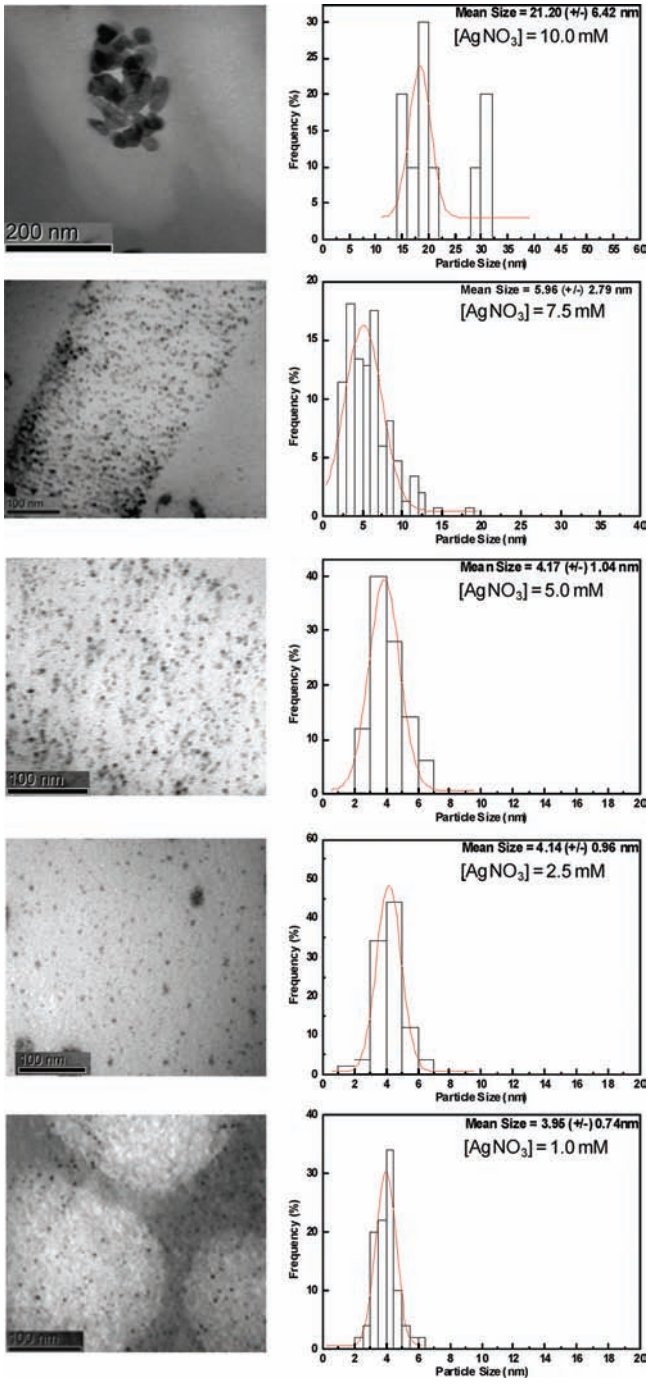

Figure 4. Transmission electron micrograph and size distribution of AgCHX nanoparticles prepared in AOT microemulsion showing the effect of $AgNO_3$ concentration. $R = 15$, water/AOT/heptane = 4.0/6.0/90.0.

small-angle neutron scattering.[48] However, the sizes of the particles derived from TEM at different R values were larger than the estimated radii of water cores for $R = 8$, 10, 12.4, and 15 (1.89, 2.25, 2.68 and 3.15 nm, respectively).

A model could be considered to illustrate the role of the reaction cage. When the particle diameter reached that of the microemulsion droplet, the surfactant molecules might adsorb on the surface of the particle formed therein. They would then act as a protective agent and restrict the growth of nanoparticles.

(48) Tamura, S.; Takeuchi, K.; Mao, G.; Csencsits, R.; Fan, L.; Otomo, T.; Saboungi, M.-L. *J. Electroanal. Chem.* **2003**, *559*, 103–109.

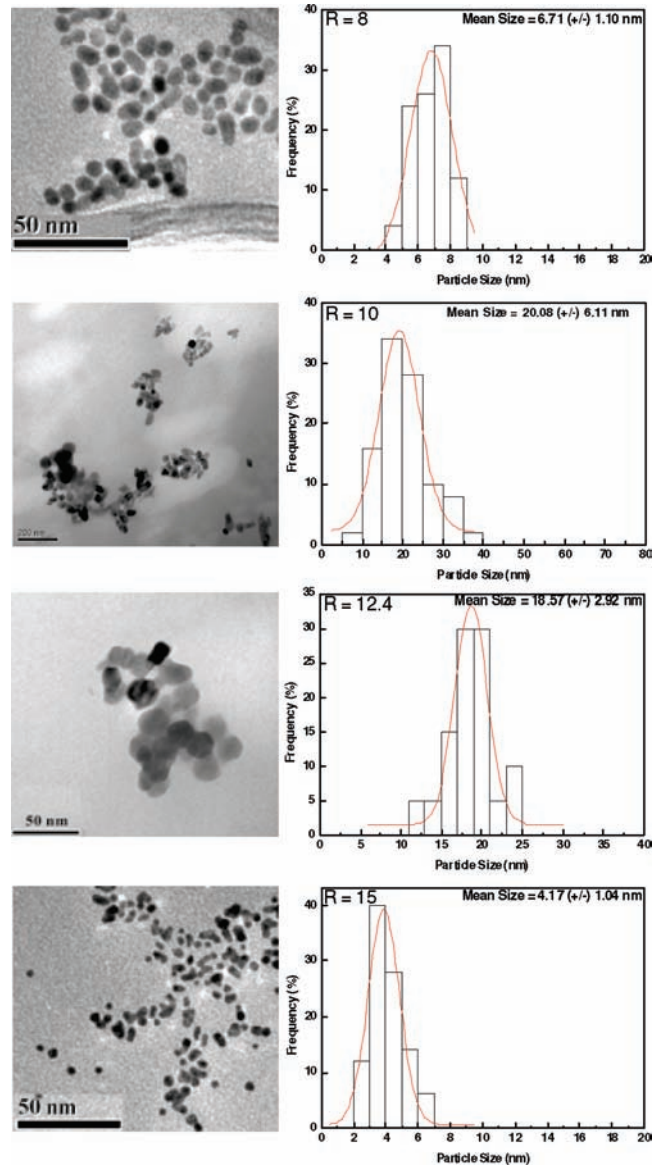

Figure 5. Transmission electron micrograph and size distribution of AgCHX nanoparticles prepared in AOT microemulsion showing the effect of the water to surfactant molar ratio ($[AgNO_3] = 5$ mM)

Due to fast exchange between the water cores, the initially formed surfactant-stabilized monometric nanoparticle nuclei grow to reach a size that corresponds to the thermodynamically most stabilized species in the presence of microemulsion. Consequently, the final nanoparticles, which are generally larger than the water cores where they were initiated, leave the water cores and form a stable colloidal suspension in the organic medium.

Figure 5 shows the TEM image and size distribution of the AgCHX nanoparticles prepared in water/AOT/heptane microemulsion at various water to surfactant molar ratios. At $R = 8$ the average particle diameter was 6.71 nm and increased to 20.08 nm at $R = 10$. This was followed by a decrease in the average particle diameter to 18.57 nm at $R = 12.4$ and then to 4.17 nm at $R = 15$ (Table 2). Water in a microemulsion medium may exist in three different forms: "bulk" water at the center of the microemulsion droplet, "bound" water that interacts with the hydrophilic part of the surfactant molecule, and monomeric or dimeric "trapped" water at the interface.[35] At low R values, all the water molecules are structured due to their interaction

Table 2. Zeta Potential and Effect of the Water to Surfactant Molar Ratio on the Occupancy Number and the Average Particle Size

R [a]	microemulsion composition (wt%) water/AOT/ heptane	AOT/heptane (wt%/wt%)	AOT/water (wt%/wt%)	$AgNO_3$ (mm)	d [b] (nm)	σ [c]	NM [d]	λ [e]	ζ [f] (mV)
8	2.0/6.0/92.0	0.07	3.0	5.0	6.71	1.10	5.1×10^{18}	6.51	44.29 ± 1.70
10	2.4/6.0/91.6	"	2.5	"	20.08	6.11	3.8×10^{18}	8.78	65.01 ± 4.88
12.4	3.0/6.0/91.0	"	2.0	"	18.57	2.92	2.8×10^{18}	12.00	66.11 ± 2.34
15	4.0/6.0/90.0	"	1.5	"	4.17	1.04	2.1×10^{18}	16.07	68.77 ± 1.65

[a] R = water to surfactant molar ratio. [b] d = number average particle diameter. [c] σ = standard deviation. [d] N_m = average number of inner water cores per prepared microemulsion. [e] λ = mean number of Ag^+ ions per water core. [f] ζ = zeta potential.

with Na^+ counterions and the strong dipole of the AOT polar group. Thus, bulk water molecules are normally not present below $R = 6-10$.[35] A ^2H NMR study on the deuterated water/AOT/heptane ternary system revealed that, with an increase in R, the bulk water of the microemulsion droplet and hence the size of the droplet increased due to the increase in the total volume of water and the concomitant decrease in the total surface of the aggregate.[35] Thus, the increase in the average diameters of AgCHX nanoparticles with the increase in R from 8 to 10 or 12.4 was expected. However, the subsequent decrease in the average particle diameter with the further increase in the diameters of microemulsion droplets ($R = 15$) apparently seemed to be inconsistent with the basic purpose of microemulsion droplets to provide a limited reaction cage for nanoparticle formation. Therefore, it is evident that, although the microemulsion droplets provide a limited microenvironment, this is not the only key factor and other factors must affect the final size of AgCHX nanoparticles formed in the water/AOT/heptane microemulsion.

Several case-specific explanations, mostly related to the concept of bound water and the rigidity of the surfactant film at the interface, were proposed, and because of the diverse nature of microemulsion systems, reactants, and reactions, no general consensus can be rationally derived. An increase in R affects several other parameters important to the formation of nanoparticles. As mentioned, the ratio of bulk water molecules to bound water molecules, or the size of the water pool, increases with an increase in R. Consequently, the average occupancy number (per microemulsion droplet) of the reacting species also increases. From another viewpoint, as shown in Table 2, the increase of water content means the decrease of AOT content or the decrease of the weight ratio of AOT to water at a constant weight ratio of AOT to heptane. The decreased weight ratio of AOT to water would lead to dilution of the interface, reducing the rigidity of the surfactant film. A more labile interface favors the rearrangement of the microemulsion droplets and results in an increased intermicellar exchange rate. When the number of ions present inside the micelle exceeds the critical nucleation number, intramicellar nucleation takes place. The number of nuclei formed is proportional to the number of micelles having a number of ions greater than the nucleation number. As shown in Table 2, the number of micelles varies within the same order of magnitude for the R values 8−15, whereas the average occupancy is lowest for the lowest R. Therefore, at lower R values, the number of nuclei formed due to intramiceller nucleation will be less than that formed at higher R values. For further nucleation, intermicellar exchange of AgCHX molecules must occur. However, due to bound water and the rigidity of the interface composed of closely packed surfactant head groups, the intermicellar exchange rate is not much favored below $R = 10$. This might refer to the condition when $r_{N_n} < r_{N_i}$. However, the average occupancy number at higher R values is higher than that at $R = 8$. Consequently, more ions will be available for growth at higher R. Therefore, particles formed at $R = 10$ will be larger than those formed at $R = 8$ (Figure 5). As R increases further, the droplet size of the microemulsion increases and the amount of bulk water molecules also increases. As a result, more of the Ag^+ ions are oxidized at the interface. Also, the polarity of the droplet and the partition coefficient of Ag^{3+} increase with the size of the droplet. These conditions facilitate greater intramicellar nucleation ($r_{N_n} > r_{N_i}$), and the resultant particle size is smaller. Moreover, at $R = 15$, the water is present as bulk water, increasing the mobility of the interface. Due to rapid collision between micelles, there will be a rapid exchange of material, leading to the formation of a larger number of micelles with a higher nuclei number. This will result in a smaller particle size, as the number of ions left for growth will be relatively low. In addition, a relatively larger number of particles with increased monodispersity will be formed.

Finally, we tested the antibacterial properties of the synthesized AgCHX toward Gram-positive and Gram-negative prokaryotes of clinical interest. Determination of minimal inhibitory concentration (MIC) is a standard microbiological technique used to evaluate the bacteriostatic activity of antimicrobial agents. The MIC values presented in Table 3 were determined using an agar dilution and a broth microdilution method.[49] AgCHX showed better bacteriostatic activity than the free ligand (CHX), silver nitrate, and silver sulfadiazine (AgSD),[50,51] even at a much lower concentration (Table 3). No antibacterial effect of the surfactant (*AOT*; test concentration 0.03−128 mg/L) was observed against the bacterial strains tested except for *Staphylococcus epidermidis*. *S. epidermidis* growth was inhibited at an AOT concentration of >64 mg/L, which is much higher than the *AOT* concentration used in the microemulsion. It is important to state that the theoretical amount of silver ions that could be released from 1 g of AgCHX is approximately 3.9 and 1.9 times lower than that from the same quantity of silver nitrate and AgSD, respectively. No difference was observed in the bacteriostatic activity and MIC of freshly prepared AgCHX and that

(49) Wiegand, I.; Hilpert, K.; Hancock, R. E. W. *Nat. Protoc.* **2008**, *3*, 163–175.
(50) Hamilton-Miller, J. M. T.; Shah, S. *Int. J. Antimicrob. Agents* **1996**, *7*, 97–99.
(51) Carr, H. S.; Wlodkowski, T. J.; Rosenkranz, H. S. *Antimicrob. Agents Chemother.* **1973**, *4*, 585–587.
(52) (a) Israelachvili, J. *Intermolecular and Surface Forces*; Academic Press: San Diego, CA, 1992. (b) Gerba, C.; Goyal, S. M.; Cech, I.; Bogdan, G. F. *Environ. Sci. Technol.* **1981**, *15*, 940–944. (c) Schafer, A.; Harms, H.; Zehnder, A. J. B. *Environ. Sci. Technol.* **1998**, *32*, 3704–3712. (d) Dickinson, R. B. *J. Colloid Interface Sci.* **1997**, *190*, 142–151. (e) Camesano, T. A.; Logan, B. E. *Environ. Sci. Technol.* **1998**, *32*, 1699–1708. (f) Elimelech, M.; O'Melia, C. R. *Langmuir* **1990**, *6*, 1153–1163. (g) Jucker, B. A.; Zehnder, A. J. B.; Harms, H. *Environ. Sci. Technol.* **1998**, *32*, 2909–2915.

Table 3. Minimal Inhibitory Concentrations (in mg/L) of AgCHX, CHX, Silver Nitrate, and Silver Sulfadiazine

	agar dilution method (values in μM)						broth dilution method (values in μM)						
	AgCHX						AgCHX						
strain	A [a]	B [b]	$AgNO_3$	AgSD [c]	$[AgNO_3]$/[AgCHX]	[AgSD]/[AgCHX]	A	B	CHX	$AgNO_3$	AgSD [e]	$[AgNO_3]$/[AgCHX]	[AgSD]/[AgCHX]
Acinetobacter calcoaceticus	1 (1.5)	1 (1.5)	32 (188)	4−16 (11−45)	125	7−30	0.12−0.25 (0.18−0.38)	0.12−0.25 (0.18−0.38)	1 (2)	16 (94)	−	247−522	−
Citrobacter freundii	4−8 (6−12)	8−16 (12−24)	16 (94)	−	8−16	−	2−4 (3−6)	2−4 (3−6)	8 (16)	4 (24)	6.25−50 (17.5−140)	4−8	3−47
Klebsiella pneumoniae	2−4 (3−6)	2−4 (3−6)	16 (94)	32−64 (90−179)	16−31	30−60	0.5 (0.75)	0.5−1 (0.75−1.5)	8 (16)	4 (24)	12.5−100 (35−280)	32	47−373
Pseudomonas aeruginosa	16 (24)	16 (24)	16 (94)	16−32 (45−90)	4	2−4	4 (6)	4 (6)	16 (32)	8 (47)	6.25−50 (17.5−140)	8	3−23
Enterococcus faecalis	4−8 (6−12)	4−8 (6−12)	32 (188)	4−64 (11−179)	16−31	2−30	1−2 (1.5−3)	2 (3)	4 (8)	16 (94)	50−100 (140−280)	31−63	47−187
Propionibacterium acne	0.25 (0.38)	0.25 (0.38)	8 (47)	−	124	−	0.06 (0.09)	0.06 (0.09)	3 (6)	4 (24)	−	267	−
Staphylococcus epidermidis	1 (1.5)	1 (1.5)	8−16 (47−94)	8−16 (22−90)	31	15−60	0.12−0.25 (0.18−0.38)	0.25 (0.38)	2 (4)	8 (47)	6.25−50 (17.5−140)	124−261	46−778
Staphylococcus aureus	2 (3)	2 (3)	32 (188)	32−128 [d] (90−358)	63	30−119	0.5 (0.75)	0.5−1 (0.75−1.5)	4 (8)	8 (47)	25−100 (70−280)	16	23−93
MRSA	1−4 (1.5−6)	1−8 (1.5−12)	32 (188)	−	31	−	ND	ND	ND	ND	−	−	−

[a] A: freshly synthesized AgCHX. [b] B: AgCHX aged for 3 months in ambient conditions. [c] From ref 50. [d] Includes 20 MRSA strains. [e] From ref 51. ND: Not done.

Table 4. MICs, MBCs, and Their Ratios for Various Disinfectants in the Broth Dilution Method

	$AgNO_3$				CHX				AgCHX			
strain	MIC (mg/L)	IC_{50} (mg/L)	MBC (mg/L)	MBC/MIC	MIC (mg/L)	IC_{50} (mg/L)	MBC (mg/L)	MBC/MIC	MIC (mg/L)	IC_{50} (mg/L)	MBC (mg/L)	MBC/MIC
Acinetobacter calcoaceticus	16	12	16−32	1−2	1	0.5	1	1	0.12	0.06	0.12−0.25	1−2
Citrobacter freundii	4	2.5	8	2	8	6	8	1	2	1	4	1
Enterococcus faecalis	16	10	16−32	1−2	4	1.5	4	1	1	0.75	2	2
Klebsiella pneumoniae	4	2.5	8	2	8	4.5	8	1	0.5	0.5	1	2
Propionibacterium acnes	4	1.2	16	4	3	2	3	1	0.06	0.02	0.06	1
Pseudomonas aeruginosa	8	2.5	8	1	16	8	32	2	4	1.5	4	1
Staphylococcus epidermidis	8	5.5	16	2	2	1	2	1	0.12−0.25	0.06	0.25	1−2
Staphylococcus aureus	8	4	16	2	4	2	4	1	0.5	0.25	0.5−1	1−2

aged for 3 months under ambient conditions. The UV−visible spectra of the synthesized nanoparticles (Figure 3b) also showed no significant difference upon storage for 3 months under ambient conditions. These results clearly indicate the excellent stability of AgCHX. It should be noted that the MICs determined using the agar dilution method were higher than that obtained from the broth microdilution method. These results further reveal the difference between the two techniques as quantitative tools to determine the antimicrobial activity of drugs. The diffusing ability of the test compound in agar might have been limited (probably because of the formation of secondary silver compounds as ionic silver is known to undergo ligand exchange reactions with biological ligands such as nucleic acids, proteins, and cell membranes) compared to that in liquid broth.[8]

Broth solution contains 0.5% sodium chloride. The lower activity of $AgNO_3$ and AgSD compared to AgCHX in liquid broth can be attributed to the precipitation of AgCl, i.e., lower availability of silver in the supernatant solutions. Therefore, we speculate that AgCHX reacts more slowly with the chloride ions than silver nitrate or AgSD in the growth medium. The contribution of the polydiguanide ligand is significant toward reducing the formation of silver chloride in the LB broth solution compared to silver nitrate. Thus, AgCHX appears to be more stable than silver nitrate in a chloride-containing medium. This is an excellent property considering the potential *in vivo* application of AgCHX.

The minimum bactericidal concentrations (MBC) were determined to evaluate the bacteriocidal properties of AgCHX. The half-maximum inhibitory concentration (IC_{50}) (Table 4) was determined by plotting the percent inhibition of bacterial growth, determined by turbidity measurement, against the concentration of the test compound. In all antimicrobial tests, CHX and silver nitrate were used as the reference standards. All test compounds, AgCHX, CHX, and $AgNO_3$, appeared to be bactericidal with MBC/MIC ratios of 1−2. The IC_{50} values of AgCHX were also much lower than those of CHX and $AgNO_3$, once again indicating the superior efficacy of AgCHX over $AgNO_3$ and CHX as an antibacterial agent.

The effectiveness of AgCHX as an antibacterial agent over a pH range (5−9) close to the physiological pH range was also evaluated by determining its MIC at different pH values (Table 5). Surprisingly, in contrast to $AgNO_3$ for which MICs increase with increased pH, the opposite trend was observed for AgCHX. Except for *C. freundii* and *P. acnes* at pH 5, the MICs of AgCHX were 4 to 500 times lower than those of $AgNO_3$ on a mole basis.

While the superior antibacterial activity of AgCHX cannot be explained unambiguously with the present data set and the

Table 5. pH Effects on the MIC of AgCHX and $AgNO_3$

strain	pH[a]	MIC (mg/L) AgCHX	MIC (mg/L) $AgNO_3$	$[AgNO_3]/[AgCHX]$
Acinetobacter calcoaceticus	5	NG[b]	NG	−
	7	0.25	16	250
	9	0.25	32	500
Citrobacter freundii	5	16	4	1
	7	4	8	8
	9	1	8	31
Klebsiella pneumoniae	5	4	8	8
	7	1	8	31
	9	0.5	8	63
Pseudomonas aeruginosa	5	0.12	2	65
	7	0.06	4	261
	9	0.06	2	130
Enterococcus faecalis	5	4	8	8
	7	2	32	63
	9	2	32	63
Propionibacterium acnes[c]	5	16	4	1
	7	8	8	4
	9	2	16	31
Staphylococcus epidermidis	5	1	4	16
	7	0.25	16	250
	9	0.12	8	261
Staphylococcus aureus	5	1	8	31
	7	1	16	63
	9	0.5	8	63

[a] pH was adjusted with dilute nitric acid for the acidic conditions and with dilute sodium hydroxide for the basic conditions. Media was autoclaved after pH adjustment. [b] NG: not grown in the control media (not supplemented with AgCHX or $AgNO_3$) under the experimental conditions.

exact mechanism needs further investigation, this probably reveals the peculiar role of high-valence cations that are efficiently dissolved in the solution where bacteria are growing, opening an avenue for increased bioavailability of active silver in the solution. This is supported by the fact that the concentration of silver in the supernatant of a chloride containing solution supplemented with AgCHX was much higher than that of a solution supplemented with equimolar $AgNO_3$.

Polydiguanides are cationic in nature and, hence, can serve as a positively charged carrier. The higher positive charge density of biguanide residues in CHX can be attributed to the relative electron-withdrawing effect of two symmetrically positioned *p*-chlorophenyl moieties. Thus, an alternative mechanism could be based on the fact that AgCHX nanoparticles serve as an improved carrier facilitating the nanoparticle agglomeration onto bacterial cells and their cellular uptake, finally leading to cell death. Bacterial adhesion or nanoparticle agglomeration on bacteria is difficult to quantify at a fundamental level as experimental measurements of factors governing the transport and adhesion of bacteria to solid surfaces (such as hydration forces,[52a] hydrophobic interactions,[52b,c] macromolecular bridging,[52d] motility,[52e] surface area and roughness,[52f] and surface characteristic of bacteria[52g]) for nanoparticle−microbe attachment are difficult. Measurement of the zeta potential and its influence on particle interaction forces has been suggested as an arguable exception to this observation.[53]

As shown in Table 1, the AgCHX nanoparticles synthesized at different *R* values have positive zeta potentials. Therefore, it may be expected that the electrostatic interactions between the synthesized AgCHX and bacterial cells will greatly influence the adsorption of these nanoparticles to bacteria cell walls and their cellular uptake. The role of electrical double-layer and van der Waals forces in particle agglomeration can be explained by classic DLVO theory. The interaction expected between a strong positively charged nanoparticle and a negative bacteria particle falls in a region where the rate of particle attachment is controlled by double-layer repulsive forces and the resulting interaction energy barrier. As the magnitude of like charges on the interacting particles decreases, the DLVO theory predicts the van der Waals force to dominate at short separation distances. This eventually results in a finite energy barrier, and particle agglomeration is no longer controlled by the energy barrier. For two oppositely charged particles, as in the case of AgCHX and bacteria, when the energy barrier disappears, the rate of agglomeration is controlled by the rate of diffusion or convective transport of bacteria or nanoparticle to the other surface. As most bacteria are negatively charged because of the predominance of the anionic groups present within the cell wall, the adsorption of positively charged nanoparticles and hence their cellular uptake should be enhanced. Therefore, as observed in this study, the positive surface potential of the synthesized AgCHX is expected to remove the repulsive double-layer interaction and result in better antibacterial efficiency. The increased agglomeration of nanoparticles onto bacteria would be in response to the increased statistical probability of collisions between a bacterium and positively charged nanoparticles where the localized charge would correspond to the minimum energy barrier. The higher surface to volume ratio of nanoparticles also ensures a larger contact surface area per unit weight of the particles with the bacterial effluent.

Conclusion

In conclusion, silver(III) polydiguanide nanoparticles were synthesized in a reverse microemulsion. This in turn demonstrated the flexibility of using a reverse microemulsion for a complexation reaction and the fabrication of essentially monodispersed nanoparticles of a higher valent metal complex. The antibacterial activity of the nanoparticles of a silver(III) complex was tested *in vitro* against four Gram (+)/(−) prokaryotes of clinical interest as well as against methicillin-resistant *Stahylococcus aureus* (MRSA) strains. The MICs of a nanocrystalline Ag(III) complex were much higher than those of $AgNO_3$ and the gold standard, silver sulfadiazine. Because of their ambient stability and high monodispersity, these nanoparticles are expected to improve the homogeneous and uniform distribution of the active agent in the host matrices of antibacterial cream or in wound dressings.

Acknowledgment. This work was supported by Korea Institute of Environmental Science and Technology (KIEST) as "The Eco-technopia 21 project" (101-091-040) and by the Korea Research Foundation Grant funded by Government of Korea (MOEHRD) (KRF-2008-314-C00239).

JA9051125

(53) (a) Limbach, L. K.; Li, Y.; Grass, R. N.; Brunner, T. J.; Hintermann, M. A.; Muller, M.; Gunther, D.; Stark, W. J. *Environ. Sci. Technol.* **2005**, *39*, 9370–9376. (b) Limbach, L. K.; Bereiter, R.; Muller, E.; Krebs, R.; Galli, R.; Stark, W. J. *Environ. Sci. Technol.* **2008**, *42*, 5828–5833.